Modeling and simulation of the vertical take off and energy consumption of a vibrating wing nano air vehicle

Le Anh Doan, Damien Faux, Samuel Dupont, Eric Cattan, Sébastien Grondel

Modeling and simulation of the vertical take off and energy consumption of a vibrating wing nano air vehicle

Le Anh Doan*, Damien Faux, Samuel Dupont, Eric Cattan, Sebastien Grondel
University of Valenciennes
IEMN, CNRS UMR-8520
Valenciennes, France
*LeAnh.Doan@etu.univ-valenciennes.fr

***Abstract*— Considering the advantages of size and robustness in performing different kinds of task, many researches on tiny flying robots have been developed in recent years. Our main objective is to develop an autonomous and bio-inspired vibrating wing nano-air-vehicle of about 3cm in wingspan relying mainly on MEMS technologies. For this purpose, a vibrating-wing nano air vehicle (VWNAV) with resonant wings using indirect actuation and concise transmission to allow large and symmetrical bending angles as well as passive wing torsion is presented. This paper introduces an innovative energy modeling of such vehicle aiming at a better comprehension of the energy transmission from energy source to wings, thus allowing future optimization of the actuation efficiency. This work also includes a dynamic model used in a closed loop control for a vertical fly of VWNAV. The results nicely demonstrate the stabilization of the system at a desired position. Considering the multiphysics nature of the prototype, a Bond Graph approach has been chosen bringing thus a unique model for the whole system.**

Keywords—MEMS, Vibrating-wing nano air vehicle, PID, Bond Graph.

I. INTRODUCTION

Inspire of the attractive aerial capacities such as hovering, backward fly and recovering after sock, very few recent prototypes have the same geometric characteristics and masses as an insect [1-5]. This could be due to undesirable surface effects such as adhesion, friction and wear [1] which makes the traditional mechanisms and macro-scale manufacturing methods become inefficient for an insect scale. To overcome the problem, a prototype with kinematics similar to those of insects using MEMS manufacturing processes has been constructed [2, 6, 7]. Large wing displacement and high power efficiency are two main objectives. In a previous paper [8], the study was focused only on the tergum actuation. This study extends the investigations on a full wings prototype providing a view of energy transmission in company with the dynamic analysis of the vibrating wing. The aerodynamic forces calculated from the wing torsion and bending motions could be used in a closed-loop vertical fly. Since the studied system combines the mechanical, the electromagnetic and the aerodynamics fields, a unique model Bond Graph formalism has been set up. This kind of formalism is widely used to model multiphysics systems and energetics efficiency. The first part of the paper is an overview of the prototype including actuation, transmission and wings. The second part answers to the question of the wing model. The aerodynamic forces are then established from retrieved wing motion. Finally, the global model is constructed with a Proportional-Integral-Derivative (PID) controller and the efficiency of the nano air vehicle is determined and discussed.

II. PRINCIPLE

A. *Prototype structure*

The prototype studied here is mainly composed of a flexible beam (tergum) with a wing at each extremity. An electromagnetic actuator glued to the thorax, positioned at the center of tergum plays a role of generating and maintaining the vibration. The compliant links transmit the vibration to the wings and affect the system efficiency. The prototype is realized in SU-8 EPOXY, which is commonly used material in MEMS technologies. Figure 1 presents an overall schematic view of the system.

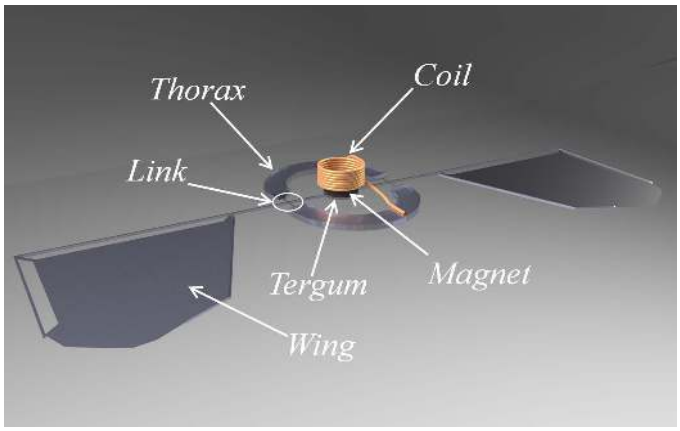

Fig. 1. Presentation of the prototype architecture.

B. *The Word Bond Graph of the prototype*

Since the prototype is considered as an incorporation of components from different engineering disciplines, Bond Graph formalism has the crucial advantage to represent it as a whole, figure 2. The model is similar to the well-known block diagram, with the major difference that the “bonds” which link the elements together represent bi-directional exchange of physical energy. Each bond depicts instantaneous flow of energy or power denoted by a pair of power variables called flow and effort. For example, the bond next to the battery block would present the flow of electrical energy and the power

variable would be the current (i_a) and the voltage (U_a), whose product is power (P_a). In like manner, the magnet displacement (ż) and the electromagnetic force (F_e) are flow and effort of the corresponding power ($P_{mechanic}$). The model of first two blocks could be found in the previous work [8].

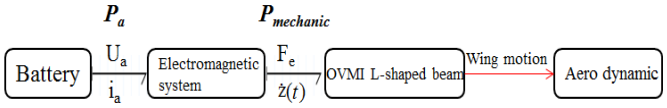

Fig. 2. Word Bond Graph of the prototype.

By understanding the dynamic phenomenon of the existing artificial wing, a modal model based on mechanical beam has been developed in the third block. The skeleton of wing is presented by an Euler Bernoulli beam as depicted in figure 3. The compliant links are as a simple supports in flexion and a springs in torsion. The coupling between flexion and torsion is simulated via the continuous conditions at the junction of the trailing edge and the leading edge.

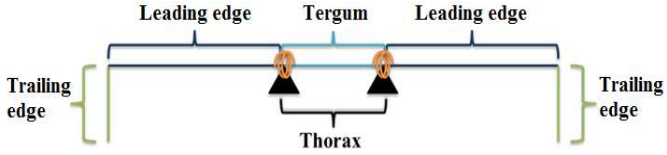

Fig. 3. Diagram of the wing skeleton.

Bending and passive torsion motions extracted from the third block comes into the last one as signals to create the aerodynamic forces. Assumption is taken here that there is a low coupling between aerodynamic forces and structural forces, which means that the kinematics is essentially due to the structural part whereas the membrane induces the aerodynamic forces. This assumption has already been validated in a previous paper [2]. In the next part, we will take a closer look at the wing model.

III. MODAL MODEL OF THE WINGS

As mentioned above, the skeleton of wings is modeled by a set of Euler-Bernoulli beams numbered from one to five as in figure 4. The vibration in bending and torsion in each beam could be expressed by the two following equations:

$$\begin{cases} EIw'''' + \rho S\ddot{w} = 0 \\ GI_0\theta'' - \rho I_0\ddot{\theta} = 0 \end{cases} \quad (1)$$

where w is the transverse displacement due to flexion, θ is the angle of torsion, EI and GI_0 are the bending and torsion stiffnesses, ρS is the mass per unit length of the beam and I_0 is the moment inertia of rotation. The lengths of leading edge, trailing edge, and the distance between two supports are L, H, and l respectively.

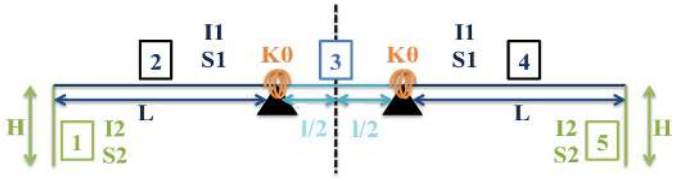

Fig. 4. Diagram of a wing of type "L"

The method of separation of variables in time and space can be used to solve equation (1) by separating the spatial and temporal function as:

$$\begin{cases} w(x,t) = \phi(x)q(t) \\ \theta(x,t) = \gamma(x)q(t) \end{cases} \quad (2)$$

which can be substituted into the flexion part of (1) to give:

$$\mu^2 \frac{\left(\phi''''(x)\right)}{\phi(x)} = -\frac{\ddot{q}(t)}{q(t)} \text{ with } \mu = \sqrt{\frac{EI}{\rho S}} \quad (3)$$

The left hand side of (3) depends on x alone while the right hand side depends on t alone. Since x and t are independent variables, both sides of (3) must be equal to the same positive constant ω^2:

$$\mu^2 \frac{\left(\phi''''(x)\right)}{\phi(x)} = -\frac{\ddot{q}(t)}{q(t)} = \omega^2 \quad (4)$$

yielding:

$$\phi''''(x) - \beta^4\phi(x) = 0 \text{ with } \beta^4 = \frac{\omega^2}{\mu^2} \quad (5)$$

$$\ddot{q}(t) + \omega^2 q(t) = 0 \quad (6)$$

the solution forms of (5) and (6) are then:

$$\phi(x) = A sin\beta x + B cos\beta x + C sinh\beta x + D cosh\beta x \quad (7)$$

$$q(t) = a sin\omega t + b cos\omega t \quad (8)$$

where A, B, C, D, a and b are unknown constants determined by the boundary and initial conditions respectively.

Inserting (2) into the torsion part of (1) we get:

$$\frac{G}{\rho}\frac{\gamma''(x)}{\gamma(x)} = \frac{\ddot{q}(t)}{q(t)} = -\omega^2 \quad (9)$$

yielding:

$$\gamma''(x) + \delta^2\beta^4\gamma(x) = 0 \text{ with } \delta = \sqrt{\frac{EI}{GS}} \quad (10)$$

the solution form of (10) is:

$$\gamma(x) = E cos(\delta\beta^2 x) + F sin(\delta\beta^2 x) \quad (11)$$

in which E and F are unknown constants determined by the boundary conditions. The following analysis applies the above solutions for each beam of the wing of type "L".

Suppose that all the segments have the same section and mechanical properties. Since the torsion has very little effect on the trailing edge (beam number 1 and 5), there are five spatial equations for flexion but only three for torsion:

$$\begin{cases} \phi_1''''(x) - \beta^4\phi_1(x) = 0 \\ \phi_2''''(x) - \beta^4\phi_2(x) = 0 \\ \phi_3''''(x) - \beta^4\phi_3(x) = 0 \\ \phi_4''''(x) - \beta^4\phi_4(x) = 0 \\ \phi_5''''(x) - \beta^4\phi_5(x) = 0 \end{cases} \quad (12)$$

$$\begin{cases} \gamma_2''(x) + \delta^2\beta^4\gamma_2(x) = 0 \\ \gamma_3''(x) + \delta^2\beta^4\gamma_3(x) = 0 \\ \gamma_4''(x) + \delta^2\beta^4\gamma_4(x) = 0 \end{cases} \quad (13)$$

It is a general mathematical principle that the number of boundary conditions necessary to determine a solution to a differential equation matches the order of the differential equation; therefore twenty-six limiting conditions are needed to solve (12) and (13). As can be seen that this set of equations has the form of the homogeneous system equations. Solve them for the value of β and the non-trivial solutions $(A_i, B_i, C_i, D_i, E_j, F_j)$, we now obtain the spatial equations of bending and torsion:

$$\phi_i(x) = A_i sin\beta x + B_i cos\beta x + C_i sinh\beta x + D_i cosh\beta x$$
$$\gamma_j(x) = E_j cos(\delta\beta^2 x) + F_j sin(\delta\beta^2 x) \quad (14)$$

for $1 \leq i \leq 5$ and $2 \leq j \leq 4$. Figure 5 shows the plot of (14) for the first mode of beam model. The membrane of the wing has been added but has no influence on the kinematics as mention previously

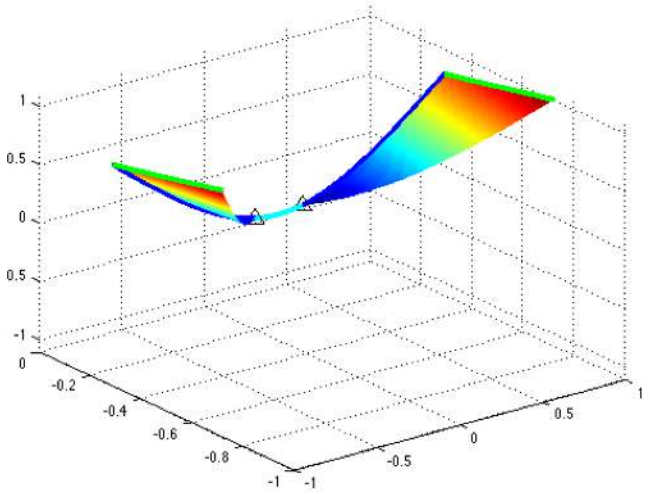

Fig. 5. First mode of beam model.

The experiments in [9] demonstrate the rightness of this model. The bending and torsion angles and also the resonance frequency derived from the simulation are close to those of the experiment. However, this system is not totally compatible with Bond Graph formalism and need a little tweaking to make itself fit. In other word, the L-shaped wing is now identified as a spring-mass-damper system. The spring stiffness ($1/k_{eq}$) and the equivalent mass (m_{eq}) are characterized in bond graph formalism by a C-element (potential energy) and a I-element (kinetic energy) respectively. The value of a R-element (dissipated energy) presents the system damping (R_{eq}) could be found in [9]. The spting stiffness k_{eq} and the equivalent mass m_{eq} are determined using the modal superposition [10] as the following integrals taken along all segments of the wing:

$$m_{eq} = \int \rho S \phi_i^2(x) dx \quad (15)$$

$$k_{eq} = \int EI \frac{d^4\phi_i(x)}{dx^4} \phi_i(x) dx \quad (16)$$

The results are summarized in the table 1 for clarity sake.

TABLE I. MECHANICAL PARAMETERS

	Used values
k_{eq}	4e-7 N/m
m_{eq}	1.4e-11 kg
R_{eq}	2e-10 kg/s
Resonance frequency	27Hz

In the mechanical domain, the 1-junction represents force balance and is a generalization of the Newton's second law. All flows of the connecting bonds at a 1-junction have the same value and the efforts sum is equal to zero:

$$m_{eq}\ddot{q}(t) + R_{eq}\dot{q}(t) + k_{eq}q(t) = F_e\phi_3(\frac{l}{2}) \quad (17)$$

Note that $F_e\phi_3(l/2)$ is the electromagnetic force acting at the middle of two supports computed directly using the modal superposition principle and q(t) is the function of time as mentioned in (2). Finally, a full prototype in Bond Graph language is shown in the figure 6.

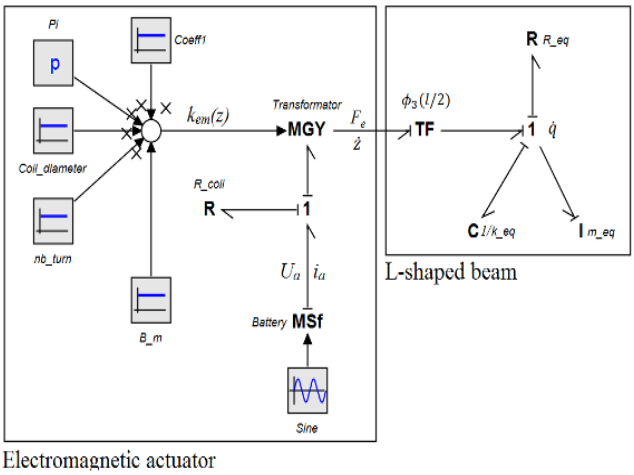

Fig. 6. Bond Graph formalism of L-shaped wing.

Recall that the electromagnetic force formula has the form:

$$F_e = B_m(z).2\pi.r.n.i_a = k_{em}(z).i_a \quad (18)$$

where $k_{em}(z)$ depicts the output signal of a block diagram MultilyDivide element which is the multiplication of the mean magnetic flux density $B_m(z)$ with the coil radius r the coil number of turn n and the 2π value. A modulated gyrator (MGY) with its gyration ratio ($k_{em}(z)$) symbolizes the transformation of electrical energy into mechanical ones. Battery is presented via a modulated source of flux i_a (MSf) and a R element stands for by coil resistor (R_{coil}). To connect the electromagnetic part with the L-shaped beam part we also need another type of transformer which is a TF element with transform ratio ($\phi_3(l/2)$). For more detail of the electromagnetic actuator refers to [8].

IV. ENERGY EVALUATION

When the current source is connected to the prototype, energy is provided to compensate the energy dissipation and maintain the wing vibration. In fact, for an electrical input power of 1mW, corresponding to a current (rms) of 80 mA and a voltage (rms) of 12.5mA, the supplying energy in one cycle is:

$$E_{cycle} = Power \times (time\ for\ cycle) \tag{19}$$

The power transformation in the electromagnetic actuator costs a major part of the input energy because of the Joules effect on the coil resistor (E_{Rcoil}). The remaining part comes into the wings and will dissipate (E_d) or store (E_s) under different ways resulting in a mechanical energy ($E_{mechanic}$). In physic and engineering, a measure of quality of an oscillatory system is its Q, defined as:

$$Q = 2\pi \frac{energy\ stored}{energy\ dissipated\ per\ cycle} \tag{20}$$

The Q factor is a dimensionless parameter that indicates the energy losses within a resonant element of a mechanical structure or an electronic circuit such as a spring or an inductor. The higher the value of Q the lower the rate of energy loss and hence the better the system is. In order to evaluate the prototype efficiency, we need to identify the two sources of energies mentioned in (20). The energy stored (E_s) corresponds to the one stored under kinematics (E_I) and potential energy (E_C). The energy dissipated (E_d) is the loss due to the resistor of coil in the electromagnetic actuator (R_{coil}) and the damping value (R_{eq}). The same analysis as in [9] revealed that E_{Rcoil} is responsible for 98% of energetics losses and therefore this work is mainly focus on the efficiency of new wing model based on remaining energy.

It is important to realize that the system is always excited to its first resonant frequency by an alternating current ($i_a=I_0\sin\omega_0 t$). In this mode, the stored energy does not change and simply moves between the stored C and I Bond graph elements. When the flow is maximum across the I bond graph element ($\dot{q}_{max}$), all the energy is in fact stored in the I element (kinetic energy):

$$E_S = \frac{1}{2}\dot{q}_{max}^2 m_{eq} \tag{21}$$

Now let's introduce the dissipated energy in the system. At each cycle, the resistor R_{eq} will dissipate energy:

$$E_d = \frac{1}{2}\frac{2\pi}{\omega_0}\dot{q}_{max}^2 R_{eq} \tag{22}$$

Substitute the results of (22) and (21) into (20), we get an encouraging value 11.5 of Q. In other words, mechanical damping (R_{eq}) dissipates only 35% of the energy rest. It also means that almost two-third of the mechanical energy is useful for generating the wings motion. The energy analysis will be the key answer for the future question of battery's capacity and mass. The compromise between them both ensures a stable and long duration of fly. Figure 7 brings to light the energy distribution.

Energy	
E_{cycle}	100%
$E_{R_{coil}}$	98%
$E_{mechanic}$	2%
E_d	0.7%
E_s	1.3%

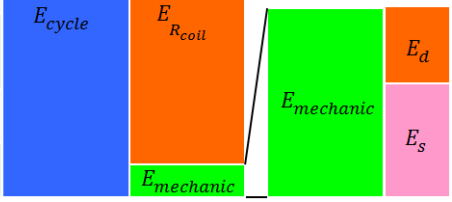

Fig. 7. Energy analysis.

V. AERODYNAMIC AND VERTICAL FLY

In nature, the flying insects achieve flight through the use of flapping wings. Robot mimicking them flap and rotate their wing periodically with sufficient large angular amplitude to perform aerial maneuvers. Flight forces with great precision are required to remain hover. The wings model developed in the section III is adapted to this requirement. In hover, the ambient air velocity is negligible, the aerodynamic forces developing only through the wing relative motion. The bending and torsion angle velocities are determined as:

$$\begin{aligned} \frac{\partial w(x,t)}{\partial x \partial x} &= \phi_2'(x) * \dot{q}(t) \\ \dot{\theta}(x,t) &= \gamma(x) * \dot{q}(t) \end{aligned} \tag{23}$$

The aerodynamic forces is commonly composed of lift and drag components, F_L and F_D. Both have the same expression, the only difference being the coefficient, C_L and C_D.

$$\begin{aligned} F_L &= \frac{1}{2}\rho \dot{w}^2 C_L(\alpha) \int r^2\, c(r) dr \\ F_D &= \frac{1}{2}\rho \dot{w}^2 C_D(\alpha) \int r^2\, c(r) dr \end{aligned} \tag{24}$$

where $\alpha = \frac{\pi}{2} - \theta$, r is radial distance from the wing root, and c is the wing chord length. Since we suppose that there is a low coupling between the aerodynamic and mechanical part, the aerodynamic block used here is instead a block diagram with the equations of aerodynamic forces inside and not a Bond Graph block. With the available wing's dimensions and the value of C_L and C_D found in [11], the output lift and drag forces are calculated by the input $\dot{q}(t)$ as in equations (23) and (24). Integrating this block to the previous Bond Graph ones; we obtain a mean lift force of 650 μ N which is enough to elevate the prototype (26 mg). One actuator prototype shows the advantage of large and symmetrical wings motion, however, that means the lift force between each wing cannot be varied for a high maneuverability of a fly. In this case, a Bond Graph model of a stable vertical takeoff flight will be demonstrated as in figure 8. In order for a fly vehicle to rise into air, the lift force (F_{Lift}) created must be at least greater than or equal to the force of gravity ($F_{Gravity}$) as shown in equation (25):

$$m_{prototype}\ddot{z} + f_{viscous} = F_{Lift} - F_{Gravity} \tag{25}$$

where z is the prototype's altitude and $m_{prototype}$ is the mass of prototype. Suppose that the prototype moves at relatively low speeds through the air, the viscous resistance $f_{viscous}$ is approximately proportional to its velocity:

$$f_{viscous} = -b\dot{z} \tag{26}$$

where b is the viscous coefficient. A 1-junction is employed to present the equation (25) as in the Vertical takeoff block.

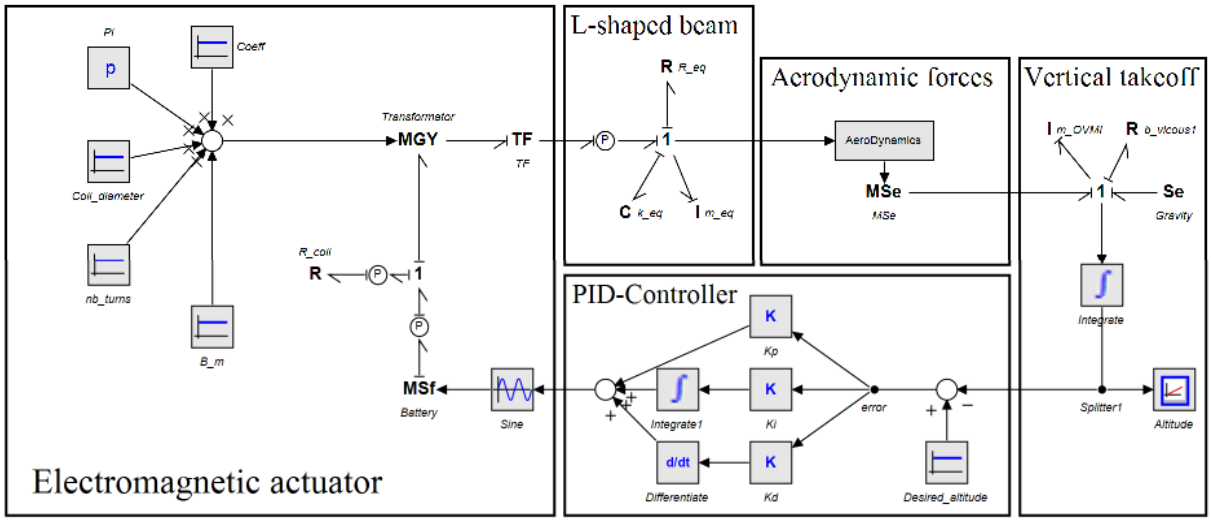

Fig. 8. Bond Graph model of closed loop fly.

A control system is modeled for this prototype using PID-controller, where the input parameter is the unstable altitude signal of vertical takeoff block (z). The altitude control result and input current are shown in figure 9. The coefficients for the proportional, integral, and derivative term (K_P, K_I and K_D) are 9, 8 and 3 respectively. For a simpler model, the mean magnetic flux density $B_m(z)$ is approximated by linear signal and the lift forces is calculated with mean value of torsional angle. Remember that the prototype always runs in its resonant mode, controlling the amplitude of input current one can have stabilized system as well as a desired altitude. The prototype reaches its desired position of 50cm after 2.5 seconds.

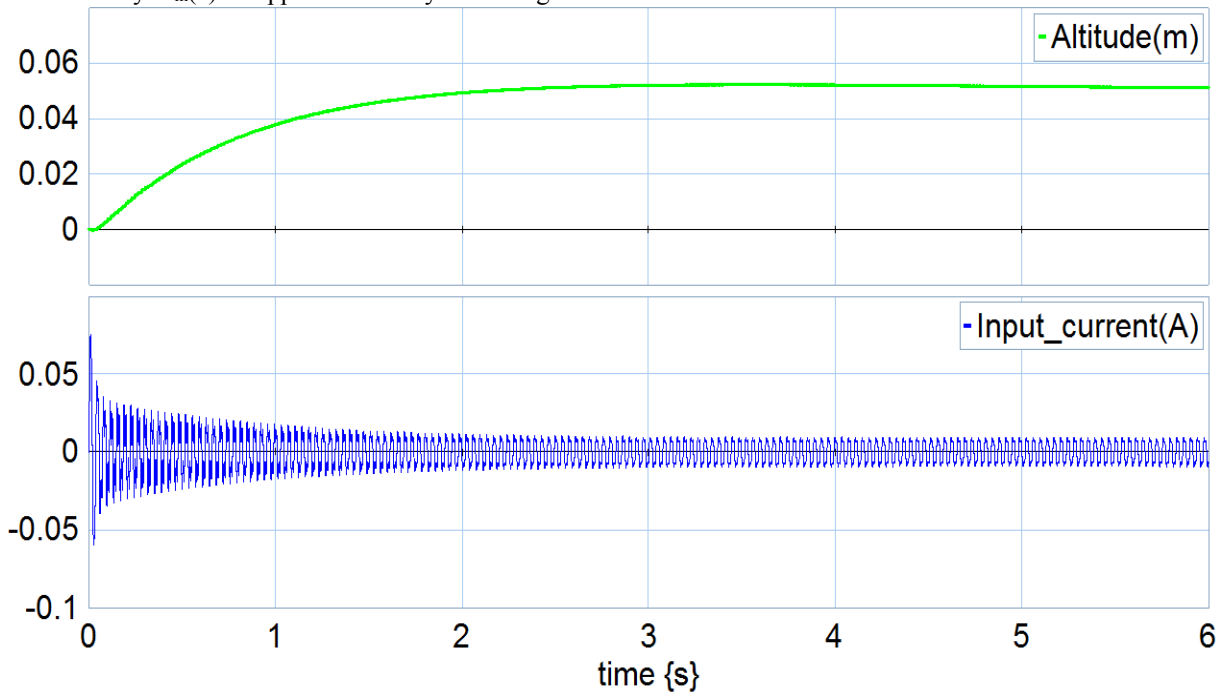

Fig. 9. Altitude control and input current.

VI. CONCLUSION AND PERSPECTIVES

This paper proposes a Bond Graph model of a VWNAV wings which has been experimentally validated and used to evaluate the whole system energy consumption. The low percentage of dissipated energy (E_d) due to mechanical damping (R_{eq}) comparing to one of the stored energy (E_S) shows a reasonable system efficiency. The vertical fly simulation reveals the prototype ability of flying up and being stable at a desired position in the vertical direction. In the next step, the strategy will be developed to reach 6 Degree Of Freedom and therefore allowing the control of VWNAV in the real space.

ACKNOWLEDGMENT

This work was realized within the ANR CLEAR-Flight project 13-0012-001 (Controlled lift for efficient flight of an Artificial Insect) which is supported by the French program ANR ASTRID.

REFERENCES

[1] Wood R J, Avadhanula S, Sahai R, Steltz E and Fearing R S 2008 Microrobot Design Using Fiber Reinforced Composites *J. Mech. Des.* **130** 052304 J. Clerk Maxwell, A Treatise on Electricity and Magnetism, 3rd ed., vol. 2. Oxford: Clarendon, 1892, pp.68-73.

[2] Dargent T, Bao X Q, Grondel S, Brun G Le, Paquet J B, Soyer C and Cattan E 2009 Micromachining of an SU-8 flapping-wing flying micro-electro-mechanical system *J. Micromechanics Microengineering* **19** 085028 K.

[3] Groen M, Bruggeman B and Remes B 2010 Improving flight performance of the flapping wing MAV DelFly II *International Micro Air Vehicle conference and competitions (IMAV 2010)* (Braunschweig, Germany).

[4] Park J and Yoon K 2007 Development of bio-mimetic composite wing structures and experimental study on flapping characteristics *Robot. Biomimetics* 25–30

[5] Pornsin-Sirirak T N, Lee S, Nassef H, Grasmeyer J, Tai Y, Ho C and Keennon M 2000 MEMS wing technology for a battery-powered ornithopter *Micro Electro Mech. Syst. 2000.* **043** 799–804

[6] Bontemps A, Vanneste T, Paquet J-B, Dietsch T, Grondel S and Cattan E 2013 Design and performance of an insect-inspired nano air vehicle *Smart Mater. Struct.* **22** 014008

[7] Pornsin-Sirirak T N T, Tai Y Y C, Nassef H and Ho C M 2001 Titanium-alloy MEMS wing technology for a micro aerial vehicle application *Sensors Actuators A Phys.* **89** 95–103

[8] Bontemps A *et al.* Modeling and evaluation of power transmission of flapping wing nano air vehicle. in *2014 IEEE/ASME 10th International Conference on Mechatronic and Embedded Systems and Applications (MESA)* 1–6 (2014). doi:10.1109/MESA.2014.6935524

[9] Bontemps A 2013 PhD thesis, Prototypage d'un Objet Volant Mimant l'Insecte (University of Valenciennes)

[10] Balachandran B, Magrab EB. Vibrations. Australia; [Clifton Park, N.Y.]: Cengage Learning; 2009.

[11] Samuel D, Sebastien G, Alexandre B, Eric C & Daniel C. Bond graph model of a flapping wing micro-air vehicle. in *2014 IEEE/ASME 10th International Conference on Mechatronic and Embedded Systems andApplications (MESA)* 1–6 (2014). doi:10.1109/MESA.2014.6935565